Supporting Information

Table of contents

S1 Experimental procedures 1
S2 X-ray crystallography 2
S3 Structural representations 4
S4 Bond valence calculations of the C_2O_4-POM. 5
S5 Characterization of the C_2O_4-POM 7
S6 Characterization of Pd/(C_2O_4-POM)@rGO 10
S7 Catalytic Hydrogenation of Olefins 14
S8 Computational details 17
S9 References 17

S1 Experimental procedures

1.1 Materials and Instruments

The precursor $K_5Na_4[P_2W_{15}(TaO_2)_3O_{59}]\cdot 17H_2O$ was synthesized according to the procedure described in our previous report.[1] $PdCl_2$ was purchased from Macklin Chemical Company. Graphene oxide (GO) (10 mg/mL) was purchased from Aladdin Chemical Company. All the other reagents were obtained commercially and used without further purification.

FT-IR analysis in ATR mode was performed by a Perkin Elmer Spectrum 400 FT-IR/FT-FIR Spectrometer equipped with ATR module in the range of 400−4000 cm^{-1} at room temperature.

UV−vis was carried out in the range of 200−800 nm on a China Cary 100 Ultraviolet spectrophotometer.

Powder X-ray diffraction (pXRD) measurements were performed on a Panalytical X'Pert3 Powder diffractometer with graphite monochromatized Cu *Kα* radiation (λ = 0.1541 nm, 40 KV, 150 mA) at 298 K.

Elemental analyses for Na, P, Ta，W and Pd were determined with a Agilent 7800(MS) ICP atomic emission spectrometer. Elemental analysis for C was performed on a Vario EL cube elemental analyzer.

Thermal analyses were performed on a Netzsch 449C thermal analyzer. The sample was heated to 800 °C with a heating rate of 5 °C/min, under an N_2 atmosphere.

Scanning electron microscope (SEM) analysis was conducted on a ZEISS GeminiSEM 300 scanning electron microscope equipped with a super energy-dispersive spectrometer (EDS).

High-resolution transmission electron microscopy (HRTEM) analysis was conducted on a FEI Talos F200x transmission electron microscope equipped with mapping. TEM samples were prepared by casting several drops of a sample solution onto copper-mesh TEM grid mounted with a holey carbon film.

Raman spectra were obtained on a LabRAMHR Evolution 4000 spectrometer with 532 nm wavelength incident laser light.

X-ray photoelectron spectroscopy (XPS) measurements were performed on Thermo Fisher Scientific ESCALAB250Xi X-ray photoelectron spectroscopy.

In situ X-ray photoelectron spectra (in situ XPS) were recorded using an ESCALAB 250Xi spectrometer (Thermo Scientific) with a monochromatic Al anode Kα radiation (1486.6 eV), and the charging effects were corrected by setting the C1s binding energy of the adventitious carbon to 284.8 eV. Prior to the measurement, the sample of **Pd/(C_2O_4-POM)@rGO** was kept in a pretreatment chamber in high purity hydrogen at room temperature for 30 min. Then the sample was directly moved to the analysis chamber without being exposed to the environment.

Nuclear magnetic resonance (NMR) spectra of ^{31}P, ^{1}H and ^{13}C were recorded on a Bruker Advance 600 MHz spectrometer. The chemical shift of ^{31}P spectrum uses 85% H_3PO_4 (δ = 0) as the internal standard, and chemical shifts were reported in parts per million (ppm, δ).

Cyclic voltammograms (CV) was recorded on an electrochemical workstation (Shanghai Chenhua Instrument Co. Ltd) at room temperature based on a three electrodes system.

1.2 Synthesis

Synthesis of $K_5Na_4[P_2W_{15}(TaO_2)_3O_{59}]\cdot 17H_2O$

$K_5Na_4[P_2W_{15}(TaO_2)_3O_{59}]\cdot 17H_2O$ was synthesized according to our previous report,[1] but with some modifications. $K_8[Ta_6O_{19}]\cdot 17H_2O$[2] (11 g, 5.5 mmol) was dissolved in an H_2O_2 solution (60 mL of 30% aqueous H_2O_2 in 800 mL of deionized water) at room temperature. HCl (75 mL, aq. 1.0 M) was added with vigorous stirring in a single addition, followed by the immediate addition of $Na_{12}[\alpha\text{-}P_2W_{15}O_{56}]\cdot 18H_2O$[3] (47.5 g, 0.011 mol, dried and ground to a fine powder before use). The resulting mixture was stirred from 30 min at room temperature and then KCl (35 g) was added. The mixture was stirred for 40 min and filtered to remove a small amount of white precipitate. Solid KCl (125 g) was added to the resulting yellow filtrate and stirred for another 40 min. The resulting yellow precipitate was collected by filtration, washed three times with ethanol (20 mL), and dried in air to give the product as a yellow powder (32 g, 55% yield based on Ta precursor). ^{31}P NMR (D_2O) δ = −10.5 (s), −14.5 (s) (referenced externally to 85% H_3PO_4).

Synthesis of $Na_2H_{38}[P_8W_{60}Ta_{12}O_{242}(C_2O_4)_4]\cdot 56H_2O$ (C_2O_4-POM)

A sample of $K_5Na_4[P_2W_{15}(TaO_2)_3O_{59}]\cdot 17H_2O$ (0.20 g, 0.04 mmol) was dissolved in 20 mL of deionized water at 80 °C. Solid $NaHSO_3$ (0.04 g, 0.38 mmol) was added with stirring until the yellow solution became colorless. Then, solid $(NH_4)_2C_2O_4$ (0.12 g, 0.84 mmol) was added. The pH of the resulting solution was adjusted to 3.0 with hydrochloric acid (1 M), and further stirred at 80 °C for 40 min. After cooled to room temperature the reaction solution was filtrated and left for evaporation. Light yellow cuboid crystal products were obtained after about one week. Yield: 0.13 g (65% based on $K_5Na_4[P_2W_{15}(TaO_2)_3O_{59}]\cdot 17H_2O$). Anal. Calcd. (%): C 0.51, Na 0.24, P 1.31, Ta 11.52, W 58.78; found C 0.58, Na 0.38, P 0.88, Ta 11.51, W 59.33. IR (KBr disks, cm^{-1}): 1608 (vw), 1405 (vw), 1078 (vw), 1012 (vw), 945 (s), 893 (s). ^{31}P NMR (D_2O) δ = -11.5 -13.6 ppm. $^{13}C\{^1H\}$ NMR (D_2O) δ =-165.42 ppm.

Synthesis of composite Pd/(C_2O_4-POM)@rGO

Pd/(C_2O_4-POM)@rGO was synthesized according to the published method[4]. 4 mL 10 mg/mL of GO dispersion was dispersed in 400 mL of high purity water and ultrasonic peel for 3 h. Adjust the pH of the solution to 2.5 using 1M $H_2C_2O_4$ solution, then 1 mL 1.2 g/mL **C_2O_4-POM** was added. The mixture was stirred for 30 minutes. 4 mL 10 mM $PdCl_2$ solution was added to the mixture and stirred for another 20 minutes. 30 mL ethanol was added and the resulting mixture was transferred to the photoreactor, flushed with nitrogen, and irradiated with a 175 W mercury lamp for 1h. The resulting black suspension was filtered and then washed with deionized water and ethanol three times to obtain the composite **Pd/(C_2O_4-POM)@rGO** (46.20 mg). The black solid material was dried in a vacuum drying oven at 100 °C for 2 h. The Pd loading amount in the composite (for GO support) was 10.64 wt% as determined by ICP-AES, the **C_2O_4-POM** loading amount in the composite (for GO support) was 13.50 wt% as determined by ICP-AES.

Synthesis of composite of Pd@rGO

Pd@rGO was synthesized according to the reported photoreduction method[5]. 4 mL 10 mg/mL of GO dispersion was dispersed in 400 mL of high purity water and ultrasonic peel for 3 h. Then 2 mL of 10 mM $PdCl_2$ solution was added. The resulting mixtrue was stirred for 30 minutes and then transferred to the photoreactor. The photoreactor was flushed with nitrogen and irradiated with a 175 W mercury lamp for 1 h. The black suspension was filtered and washed with deionized water and ethanol three times to obtain the composite **Pd@rGO**. The black solid was dried in a vacuum drying oven at 100 °C for 2 h. The Pd loading amount in the composite (for GO support) was 12.56 wt% as determined by ICP-AES.

S2 X-ray crystallography

Single crystal XRD analysis of **C_2O_4-POM** was recorded on an Agilent SuperNova Dual diffractometer using graphite-monochromated Mo *Kα* radiation, λ = 0.71073 Å. The linear absorption coefficients, scattering factors for the atoms, and anomalous dispersion corrections were taken from the International Tables for X-Ray Crystallography. Empirical absorption corrections were applied. Structures were solved using direct methods (SHELXT)[6] and refined by full-matrix least-squares (SHELXL) interfaced with the program OLEX2.[7] Anisotropic thermal parameters were used to refine all non-hydrogen atoms, with the exception for a few oxygen atoms. Those hydrogen atoms attached to lattice water molecules were not located. Crystallization water molecules were estimated by thermogravimetry and only partial of them were achieved with the X-ray structure analysis. The crystal data and structure refinement results are summarized in Table S1. Further details on the crystal structure investigations can be obtained free of charge from The Cambridge Crystallographic Data Centre via https://www.ccdc.cam.ac.uk/structures/ by quoting the depository numbers CCDC-2321884 (**C_2O_4-POM**).

Table S1. Crystal data and structural refinements.[a]

Compound	**C_2O_4-POM**
Formula	$C_8Na_2O_{283}P_8Ta_{12}W_{60}$
Formula weight (g·mol^{-1})	18120.22
T (K)	150(10)
Wavelength (Å)	1.54184
Crystal	monoclinic
Space group	$P2_1/n$
a (Å)	37.0584(4)
b (Å)	24.8913(3)
c (Å)	37.1568(4)
α (˚)	90
β (˚)	93.1020(10)
γ (˚)	90
V (Å^3)	34224.4(7)
Z	4
D_{calc} (mg m^{-3})	3.517
μ (mm^{-1})	24.020
F (000)	31080.0
Crystal size (mm^3)	0.15 × 0.09 × 0.09
Goodness-of-fit on F^2	0.981
Final *R* indices	R_1 = 0.0850
[I >2σ(I)][a]	wR_2 = 0.2057
R indices[a]	R_1 = 0.1431
(all data)	wR_2= 0.2341

[a] $R_1=\sum||F_o|-|F_c||/\sum|F_o|$; $wR_2 = \{\sum[w(F_o^2-F_c^2)^2]/\sum[w(F_o^2)^2]\}^{1/2}$

S3 Structural representations

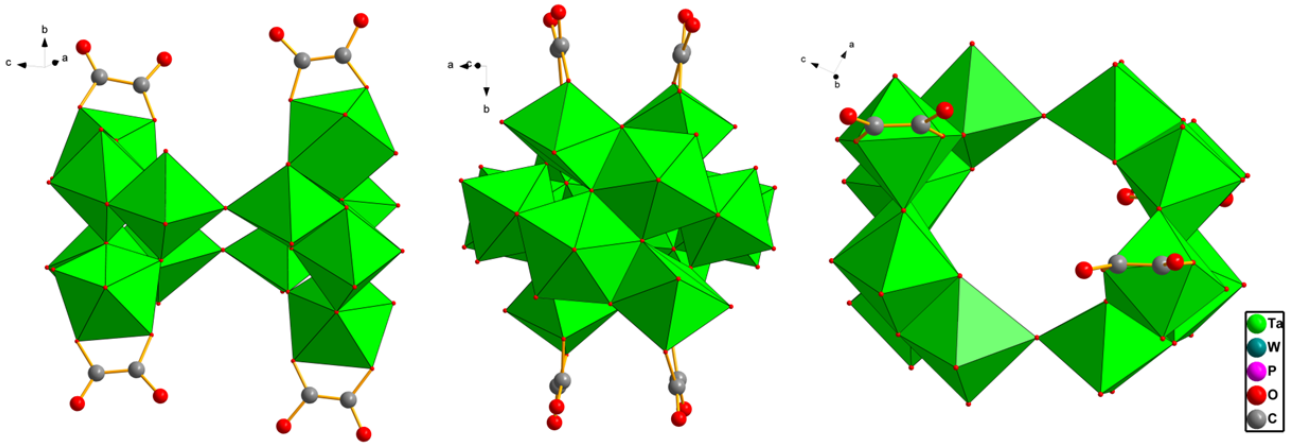

Figure S1. Mixed polyhedral/ball-and-stick representations of the central $\{Ta_{12}O_{42}(HC_2O_4)\}$ cluster in **C_2O_4-POM**.

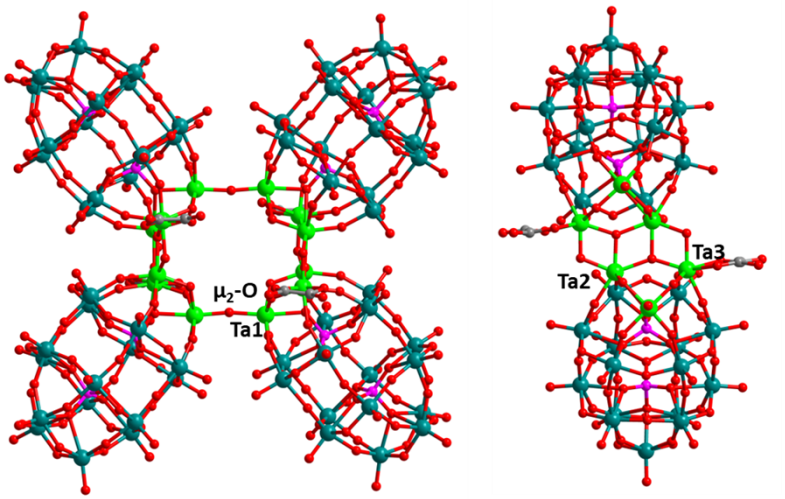

Figure S2. Ball-and-stick representation of **C_2O_4-POM**, highlighting the coordination environment of Ta1 and the μ_2-O (left) and a half of **C_2O_4-POM** highlighting the coordination of Ta2 and Ta3 (right).

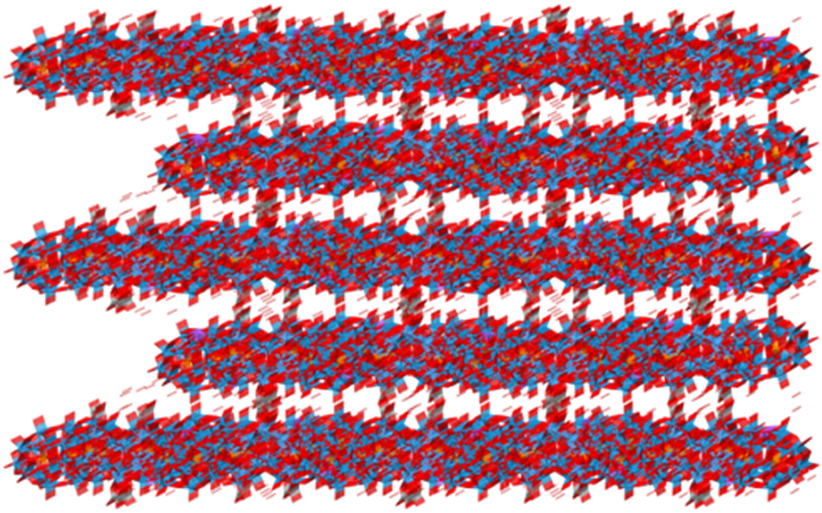

Figure S3. Ball-and-stick representation of 2D layer for **C_2O_4-POM**.

S4 Bond valence calculations of the C_2O_4-POM.

Table S2. Bond valence calculations of select O atoms of the **C_2O_4-POM**.

Atom	Bond	Distance/Å	Bond Valence	Bond Valence Sum (BVS)
O1	O1-Ta3	1.935	0.960	2.178
	O1-Ta4	1.847	1.218	
O2	O2-Ta11	1.870	1.145	2.183
	O2-Ta8	1.906	1.039	
O3	O3-Ta7	1.895	1.070	1.839
	O3-Ta8	2.017	0.769	
O5	O5-Ta5	1.952	0.917	1.839
	O5-Ta7	1.952	0.917	
O6	O6-Ta5	1.994	0.819	2.212
	O6-Ta6	2.064	0.678	
	O6-Ta7	2.044	0.715	
O7	O7-Ta6	2.026	0.751	2.235
	O7-Ta7	2.100	0.615	
	O7-Ta9	1.972	0.869	
O8	O8-Ta4	1.921	0.997	1.905
	O8-Ta5	1.956	0.907	
O9	O9-Ta4	1.936	0.958	2.010
	O9-Ta6	1.901	1.053	
O11	O11-Ta6	1.931	0.971	1.734
	O11-Ta9	2.020	0.763	
O17	O17-C6	1.331	1.205	1.766
	O17-Ta5	2.134	0.561	
O18	O18-C5	1.350	1.145	1.709
	O18-Ta5	2.132	0.564	
O19	O19-C6	1.278	1.391	1.391
O20	O20-C5	1.251	1.495	1.495
O21	O21-Ta2	1.966	0.883	1.810
	O21-Ta12	1.948	0.927	
O22	O22-Ta2	2.044	0.715	2.217
	O22-Ta10	2.096	0.621	
	O22-Ta12	1.967	0.881	
O23	O23-Ta1	1.892	1.079	1.871
	O23-Ta10	2.006	0.793	
O24	O24-Ta1	2.024	0.755	2.212
	O24-Ta2	2.071	0.665	
	O24-Ta10	2.006	0.793	
O25	O25-Ta10	1.918	1.005	1.844
	O25-Ta11	1.985	0.839	
O26	O26-Ta2	1.915	1.014	1.869
	O26-Ta3	1.978	0.855	
O27	O27-Ta1	2.117	0.587	1.571
	O27-C3	1.406	0.984	
O28	O28-Ta1	2.158	0.526	1.734
	O28-C4	1.330	1.208	
O29	O29-C4	1.328	1.215	1.215
O59	O59-C1	1.181	1.807	1.807
O89	O89-C3	1.235	1.562	1.562
O90	O90-Ta12	2.163	0.519	1.861
	O90-C7	1.291	1.343	
O91	O91-Ta12	2.227	0.436	1.698
	O91-C8	1.314	1.262	
O07X	O07X-Ta9	2.190	0.482	1.596
	O07X-C1	1.360	1.114	
O06B	O06B-Ta9	2.130	0.567	1.730
	O06B-C2	1.344	1.163	
O92	O92-C8	1.272	1.413	1.413
O94	O94-C7	1.362	1.108	1.108
O96	O96-Ta3	1.866	1.157	1.963
	O96-Ta1	2.000	0.806	
O108	O108-C2	1.241	1.537	1.537

Table S3. Bond valence calculations of Ta atoms of the **C_2O_4-POM**.

Atom	Bond	Distance/Å	Bond Valence	Bond Valence Sum (BVS)
Ta1	Ta1-O23	1.892	1.079	5.258
	Ta1-O24	2.024	0.755	
	Ta1-O27	2.117	0.587	
	Ta1-O28	2.158	0.526	
	Ta1-O47	2.031	0.741	
	Ta1-O48	2.019	0.765	
	Ta1-O96	2.000	0.806	
Ta2	Ta2-O21	1.966	0.883	5.233
	Ta2-O22	2.044	0.715	
	Ta2-O24	2.071	0.665	
	Ta2-O26	1.915	1.014	
	Ta2-O45	2.021	0.761	
	Ta2-O46	1.947	0.930	
	Ta2-O97	2.411	0.265	
Ta3	Ta3-O1	1.935	0.960	5.129
	Ta3-O26	1.978	0.855	
	Ta3-O43	2.022	0.759	
	Ta3-O44	1.986	0.837	
	Ta3-O96	1.866	1.157	
	Ta3-O97	2.134	0.561	
Ta4	Ta4-O1	1.847	1.218	5.204
	Ta4-O8	1.921	0.997	
	Ta4-O9	1.936	0.958	
	Ta4-O15	2.051	0.702	
	Ta4-O16	2.014	0.776	
	Ta4-O103	2.139	0.553	
Ta5	Ta5-O5	1.952	0.917	5.185
	Ta5-O6	1.994	0.819	
	Ta5-O8	1.956	0.907	
	Ta5-O10	2.067	0.672	
	Ta5-O14	2.029	0.745	
	Ta5-O17	2.134	0.561	
	Ta5-O18	2.132	0.564	
Ta6	Ta6-O6	2.064	0.678	5.169
	Ta6-O7	2.026	0.751	
	Ta6-O9	1.901	1.053	
	Ta6-O11	1.931	0.971	
	Ta6-O12	1.980	0.850	
	Ta6-O13	2.089	0.633	
	Ta6-O103	2.459	0.233	
Ta7	Ta7-O3	1.895	1.070	5.258
	Ta7-O5	1.952	0.917	
	Ta7-O6	2.044	0.715	
	Ta7-O7	2.100	0.615	
	Ta7-O38	1.955	0.910	
	Ta7-O39	2.004	0.797	
	Ta7-O53	2.457	0.234	
Ta8	Ta8-O2	1.906	1.039	4.960
	Ta8-O3	2.017	0.769	
	Ta8-O4	1.914	1.016	
	Ta8-O40	2.018	0.767	
	Ta8-O41	1.993	0.821	
	Ta8-O53	2.143	0.547	
Ta9	Ta9-O4	1.946	0.932	5.182
	Ta9-O7	1.972	0.869	
	Ta9-O11	2.020	0.763	
	Ta9-O36	2.004	0.797	
	Ta9-O37	2.016	0.771	
	Ta9-O06B	2.130	0.567	
	Ta9-O07X	2.190	0.482	
	Ta10-O22	2.096	0.621	
	Ta10-O23	2.006	0.793	

Ta10	Ta10-O24	2.006	0.793	5.193
	Ta10-O25	1.918	1.005	
	Ta10-O31	1.909	1.030	
	Ta10-O32	2.041	0.721	
	Ta10-O105	2.465	0.229	
Ta11	Ta11-O2	1.870	1.145	5.530
	Ta11-O25	1.985	0.839	
	Ta11-O30	1.899	1.058	
	Ta11-O33	2.005	0.795	
	Ta11-O49	1.869	1.148	
	Ta11-O105	2.144	0.546	
Ta12	Ta12-O21	1.948	0.927	5.367
	Ta12-O22	1.967	0.881	
	Ta12-O34	1.980	0.850	
	Ta12-O35	1.974	0.864	
	Ta12-O49	1.963	0.890	
	Ta12-O90	2.163	0.519	
	Ta12-O91	2.227	0.436	

S5 Characterization of the C_2O_4-POM

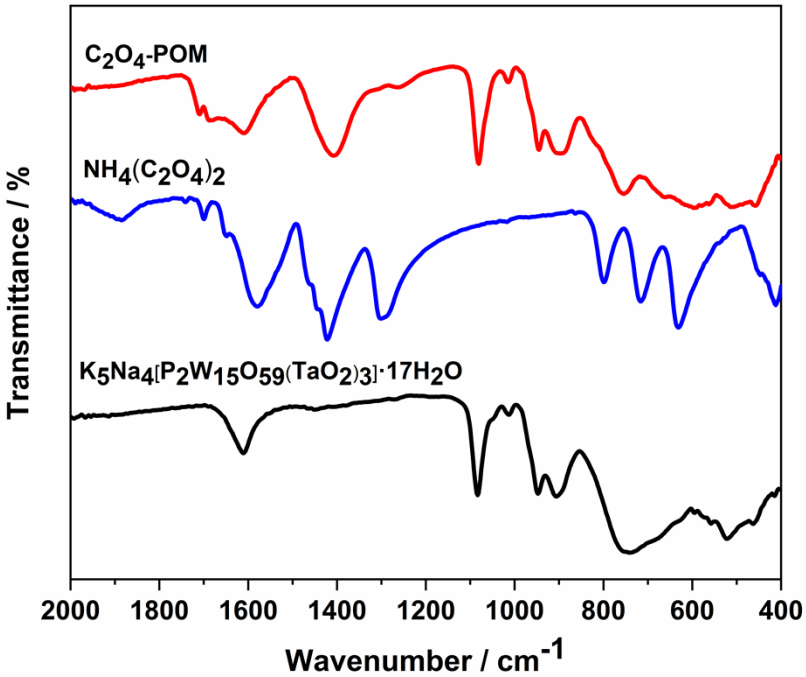

Figure S4. IR spectra of **C_2O_4-POM**.

The strong signal peak of **C_2O_4-POM** at 1611 cm^{-1} can refer to the stretching vibration of lattice water and coordination water molecules. The characteristic signal peaks of C_2O_4-POM at 1085 cm^{-1}, 1026 cm^{-1}, 951 cm^{-1}, 901 $cm^{-1}$and 760 cm^{-1} . It can be attributed to the stretching vibration of Vas(P-O_a), Vas(W-O_t), Vas(W-O_b-W), Vas(W-O_C-W) in Dawson type anions. 1405 cm^{-1} and 1608 cm^{-1} are attributed to symmetric and antisymmetric stretching vibrations of C=O, respectively.

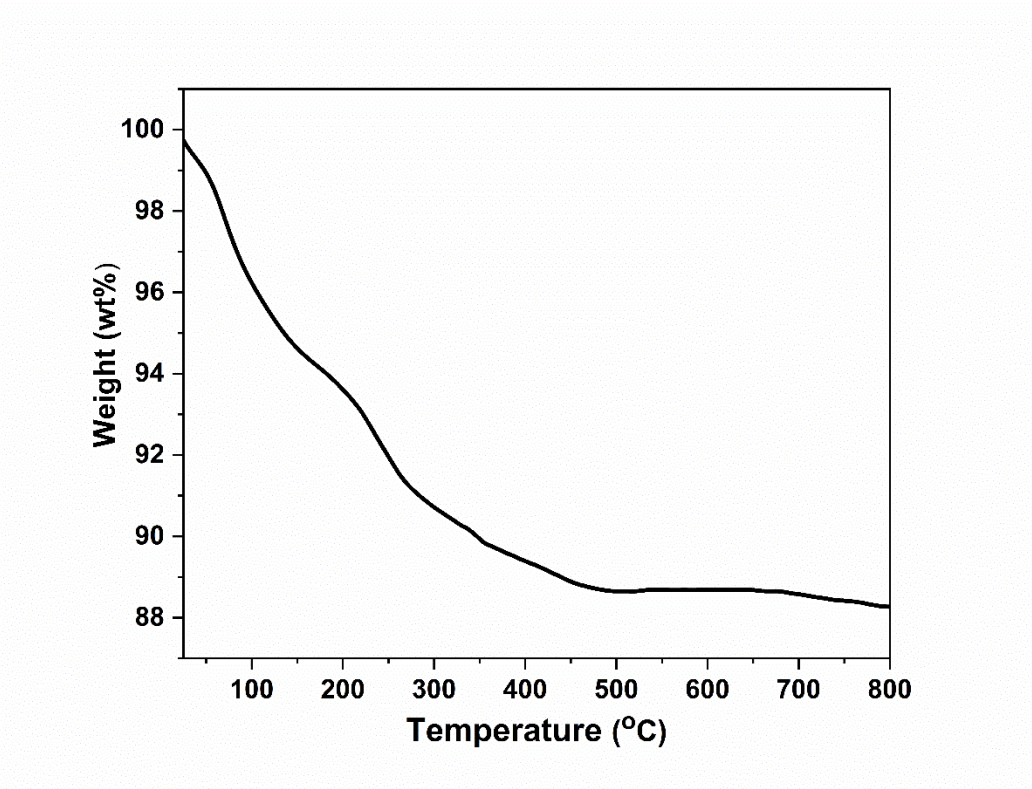

Figure S5. The TGA curves of **C_2O_4-POM** measured in N_2 from 25 °C to 800 °C.

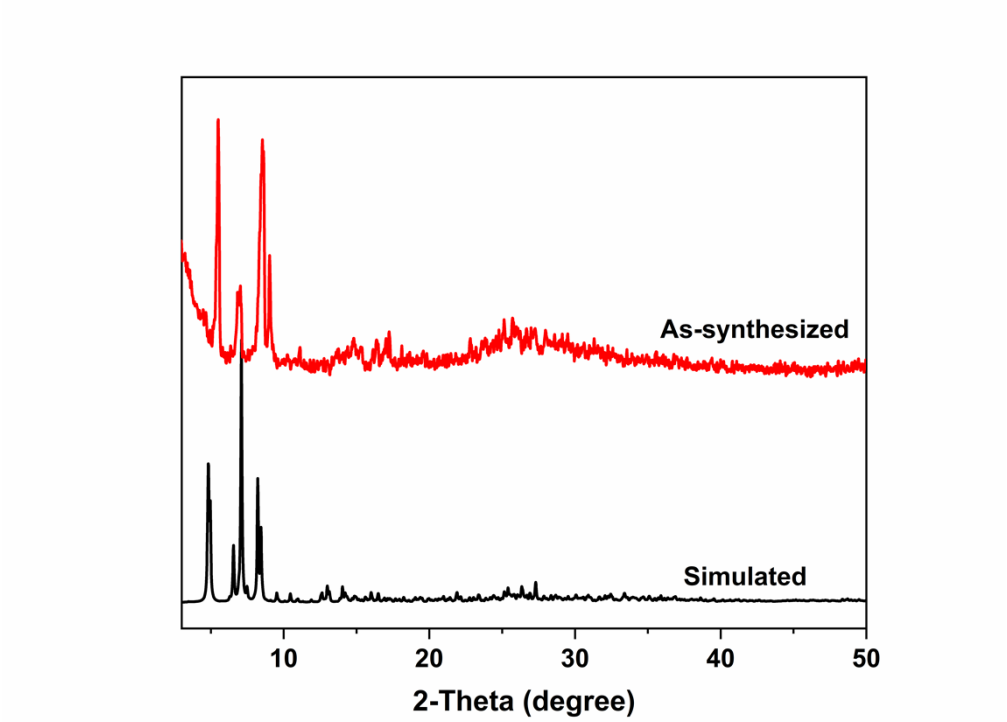

Figure S6. Simulated (black) and as-synthesized (red) PXRD patterns of **C_2O_4-POM**.

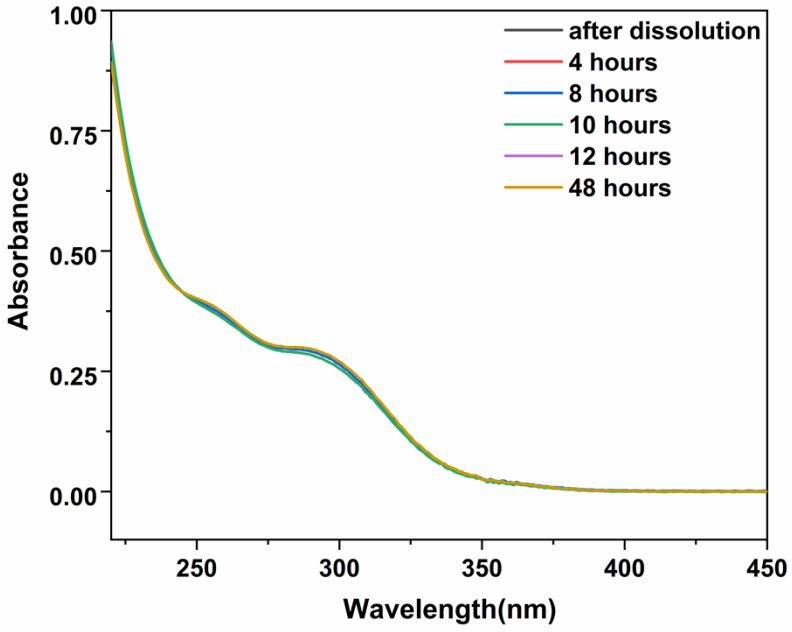

Figure S7. UV-vis absorption spectra of **C_2O_4-POM** in acidic solution (pH = 2.5).

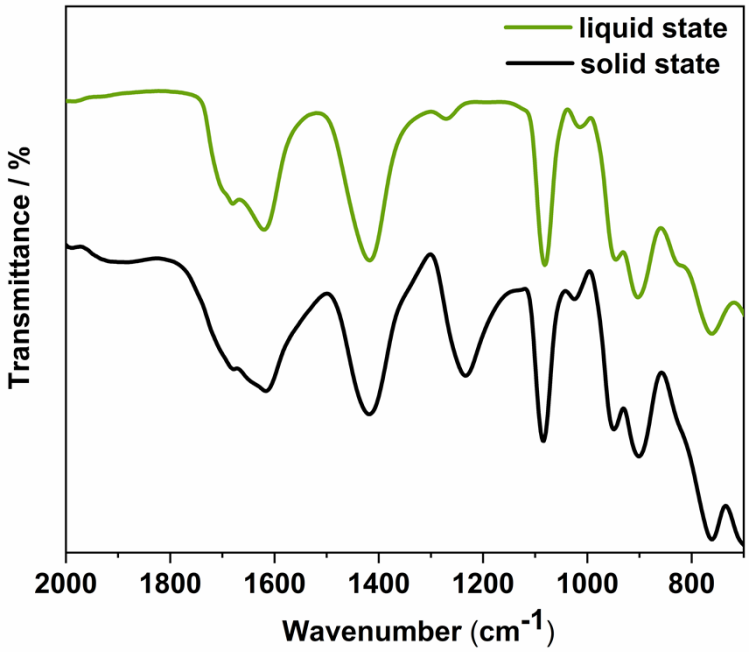

Figure S8. IR spectra of **C_2O_4-POM** in acidic solution (pH = 2.5) and solid state.

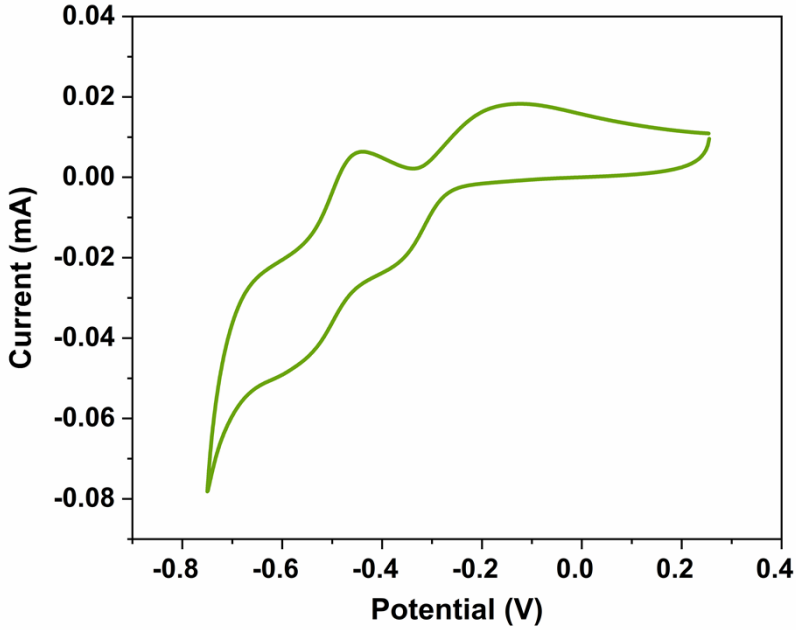

Figure S9. Cyclic voltammogram of **C_2O_4-POM** in 0.1 M HCl (1.65 mM) at 10 mVs^{-1}. The working electrode was glassy carbon, counter electrode was platinum filament, and the reference electrode was Ag/AgCl.

S6 Characterization of Pd/(C_2O_4-POM)@rGO

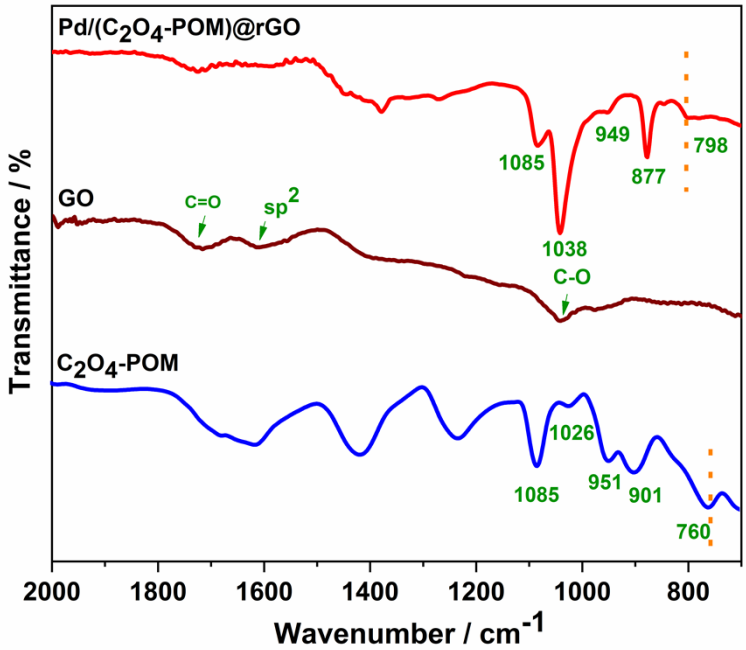

Figure S10. IR spectra of **Pd/(C_2O_4-POM)@rGO.**

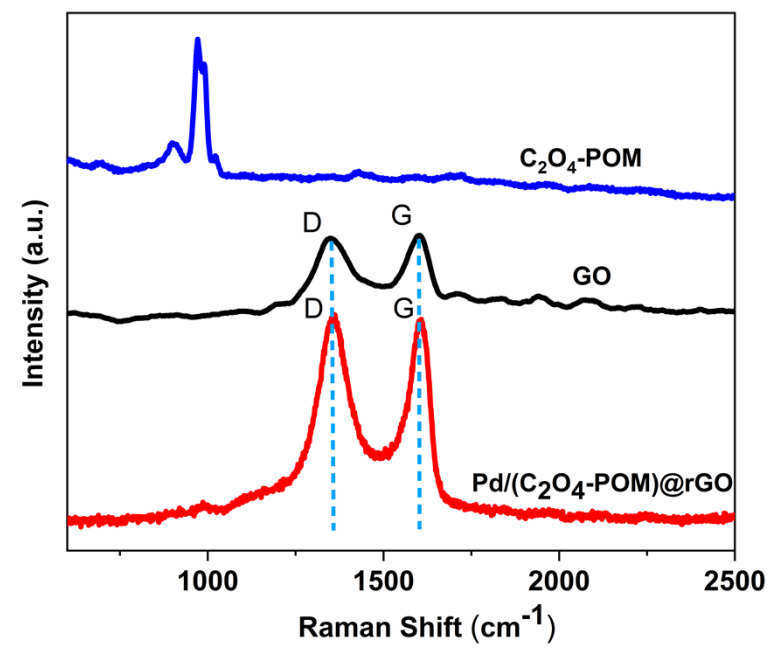

Figure S11. Raman spectra of **GO** and **Pd/(C_2O_4-POM)@rGO**.

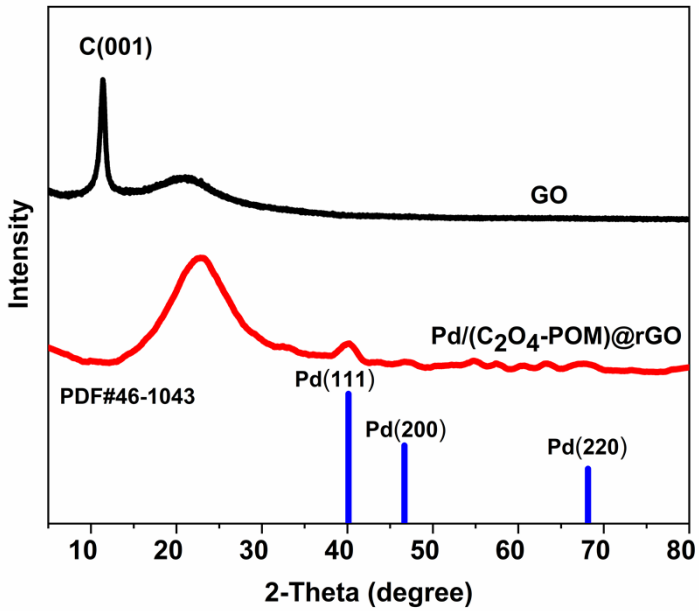

Figure S12. XRD spectra of **GO**, **Pd/(C_2O_4-POM)@rGO** and Pd NPs.

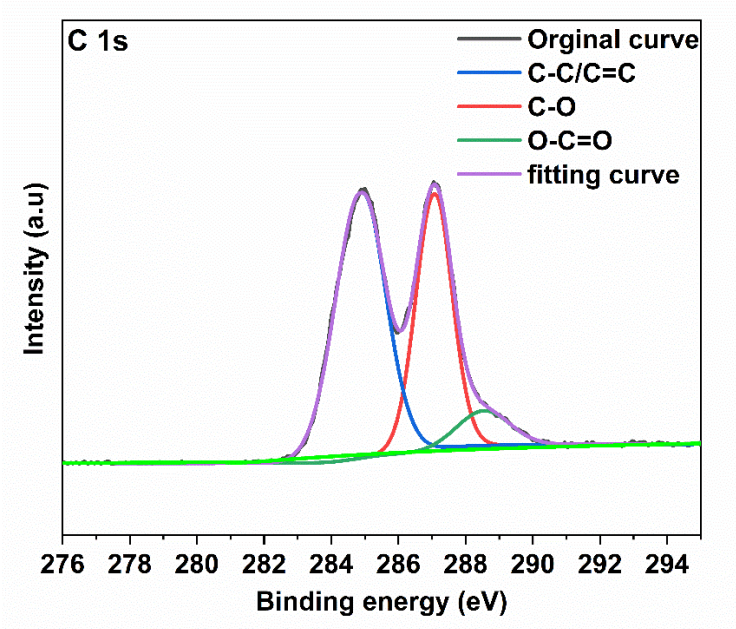

Figure S13. XPS spectra of C 1s of **GO**.

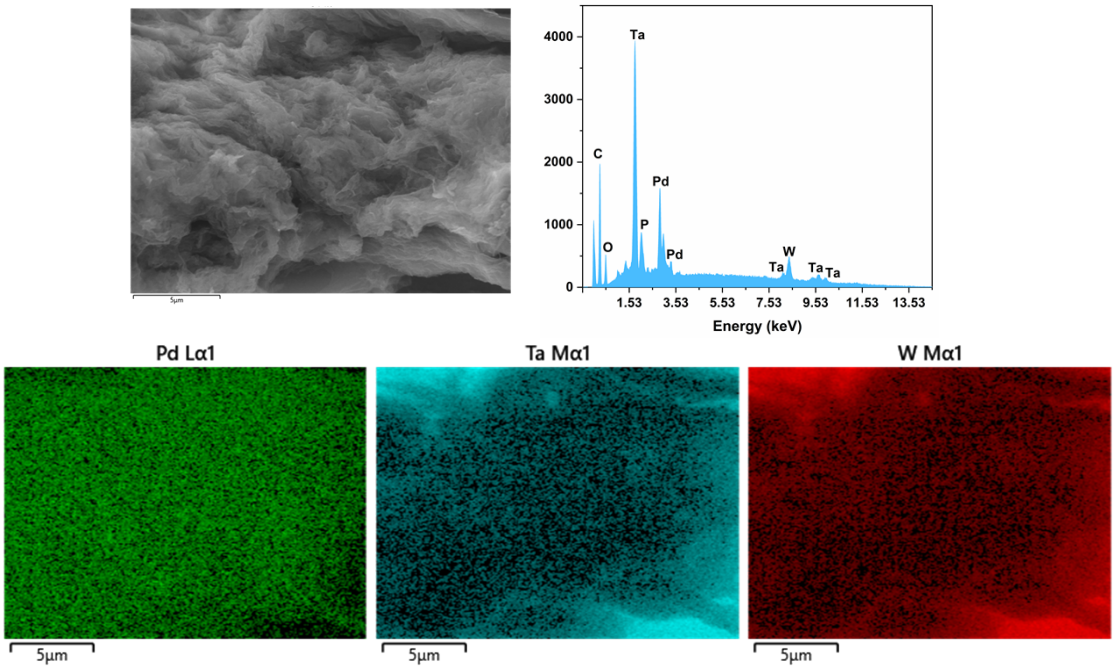

Figure S14. SEM-EDX spectra and the elemental mapping of Pd, W and Ta for **Pd/(C_2O_4-POM)@rGO**.

Table S4. Binding energy and percentage of various components for **Pd/(C_2O_4-POM)@rGO** before and after exposure to H_2 as determined by XPS analysis.

Sample	Binding Energy/eV	Relative Content [%]
before H_2 exposure		
W^{6+}	36.2	100
	38.3	
after H_2 exposure		
W^{5+}	34.7	73.2
	36.8	
$W^{\delta+}$	33.8	26.8
	31.8	
before H_2 exposure		
Pd^0	335.3	44.9
	340.6	
Pd^{2+}	337.2	55.1
	342.4	
after H_2 exposure		
Pd^0	335.7	100
	340.9	
before H_2 exposure		
-OH	532.2	43.0
$-OH_2$	535.2	5.18
O_{latt}	531.1	51. 8
after H_2 exposure		
-OH	531.6	87.7
$-OH_2$	535.8	5.76
O_{latt}	529.8	6.6

[a] Estimated based on the area of each pair of peaks

S7 Catalytic Hydrogenation of Olefins

Hydrogenation of Olefins：Catalysts were introduced in a reaction tube with a stirrer bar and sealed with a silicone septum. After replacing the air with Hydrogen, the substrate (0.2 mmol) and solvent (2 mL) were introduced in the tube. The reaction was performed at room temperature (r.t.) under H_2 (1 bar). Yields were determined by GC-MS. Solid reaction products were recovered by centrifugation and filtering to remove the catalyst, followed by rotary evaporation to remove the solvent.

Table S5. Optimization of the conditions for hydrogenation of olefins [a].

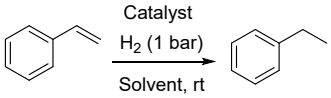

Entry	Catalyst	Solvent	Time (min)	Yield (%)
1	**Pd/(C_2O_4-POM)@rGO**	Ethanol	40	84
2	**Pd/(C_2O_4-POM)@rGO**	Acetone	40	63
3	**Pd/(C_2O_4-POM)@rGO**	Toluene	40	28
4	**Pd/(C_2O_4-POM)@rGO**	Tetrahydrofuran	40	80
5	**Pd/(C_2O_4-POM)@rGO**	Acetonitrile	40	99

[a]Reaction condition: 0.2 mmol substrates, room temperature, 2 mL solvent, and 1 atm H_2 for 40 min, 4.8 mg **Pd/(C_2O_4-POM)@rGO** catalyst (5 μmol Pd), Yields Were determined by GC-MS.

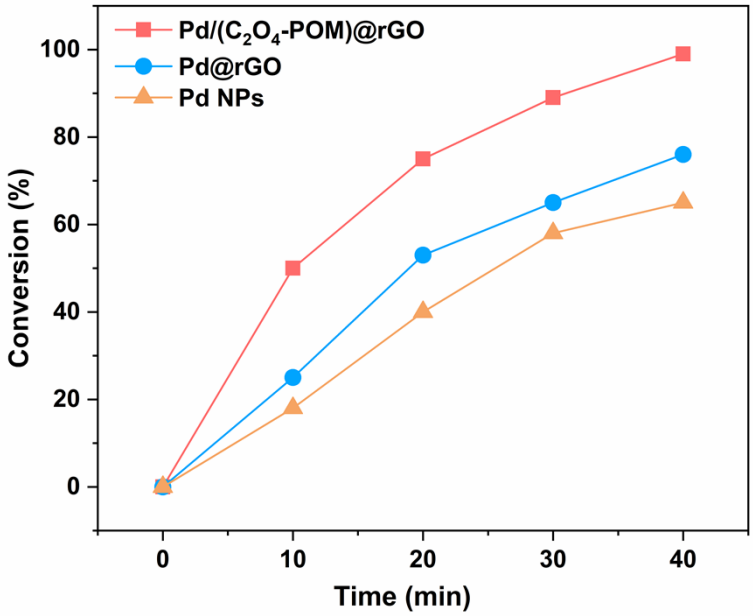

Figure S15. Comparison of the catalytic activity and Styrene hydrogenation conversion over time for **Pd/(C_2O_4-POM)@rGO**, **Pd@rGO, Pd NPs**. Reaction conditions: 0.2 mmol styrene, room temperature, 2 mL CH_3CN, and 1 atm H_2 for 40 min. Catalyst: 4.8 mg **Pd/(C_2O_4-POM)@rGO** Catalyst (5 μmol Pd), 4.2 mg **Pd@rGO** Catalyst (5 μmol Pd), 0.53 mg **Pd NPs** Catalyst (5 μmol Pd).

Table S6 Catalytic reaction of olefins derivatives by **Pd/(C_2O_4-POM)@rGO**.

Entry	Substrate	Product	Yield(%)
1	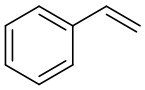	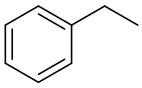	>99%
2	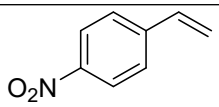	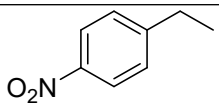	>99%
3	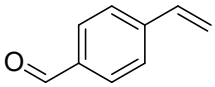	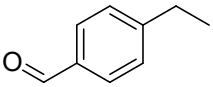	>99%
4	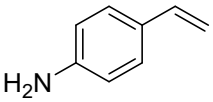	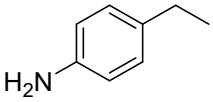	>99%
5	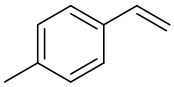	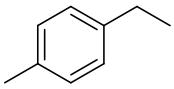	>99%
6	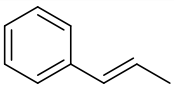	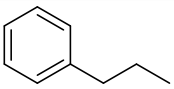	>99%
7	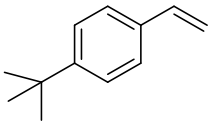	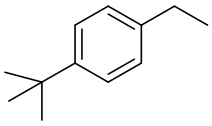	>99%
8	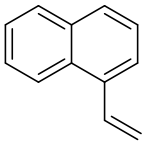	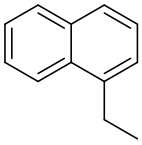	>99%
9	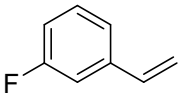	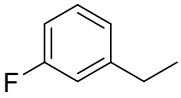	>99%
10	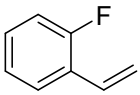	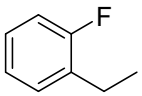	>99%
11	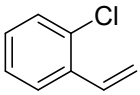	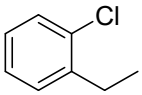	>99%
12	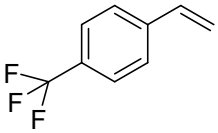	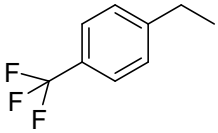	>99%
13	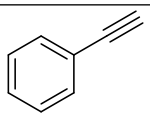	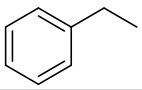	>99%

Reaction condition: 4.8 mg **Pd/(C_2O_4-POM)@rGO** Catalyst (5 μmol Pd), 0.2 mmol substrates, room temperature, 2 mL of CH_3CN solvent, and 1 atm H_2 for 1 h.

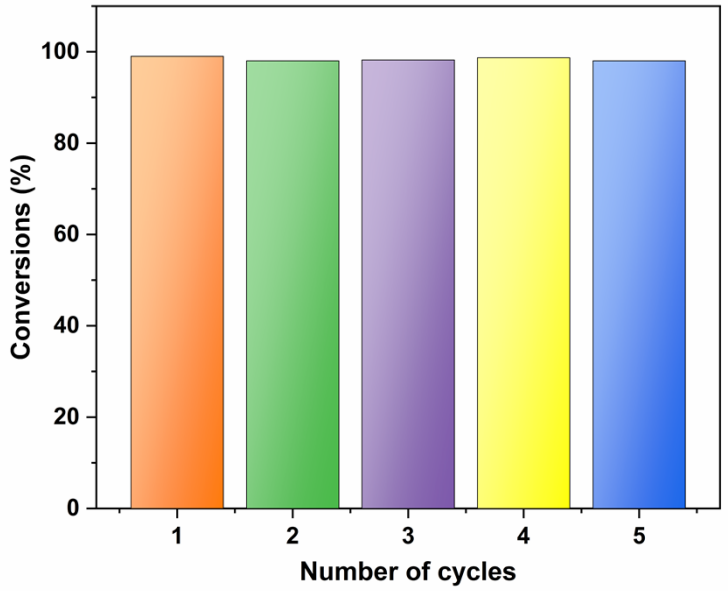

Figure S16. Recyclability of **Pd/(C_2O_4-POM)@rGO** for the hydrogenation of olefins.

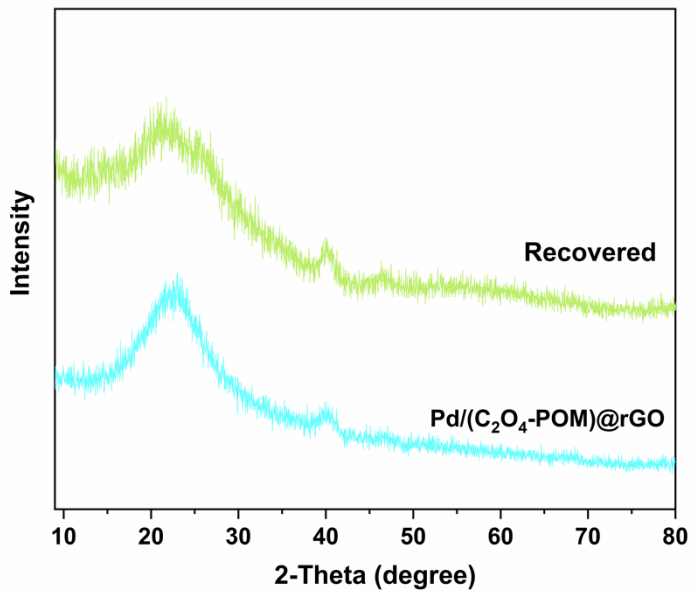

Figure S17. Powder XRD patterns of **Pd/(C_2O_4-POM)@rGO** before and after catalysis.

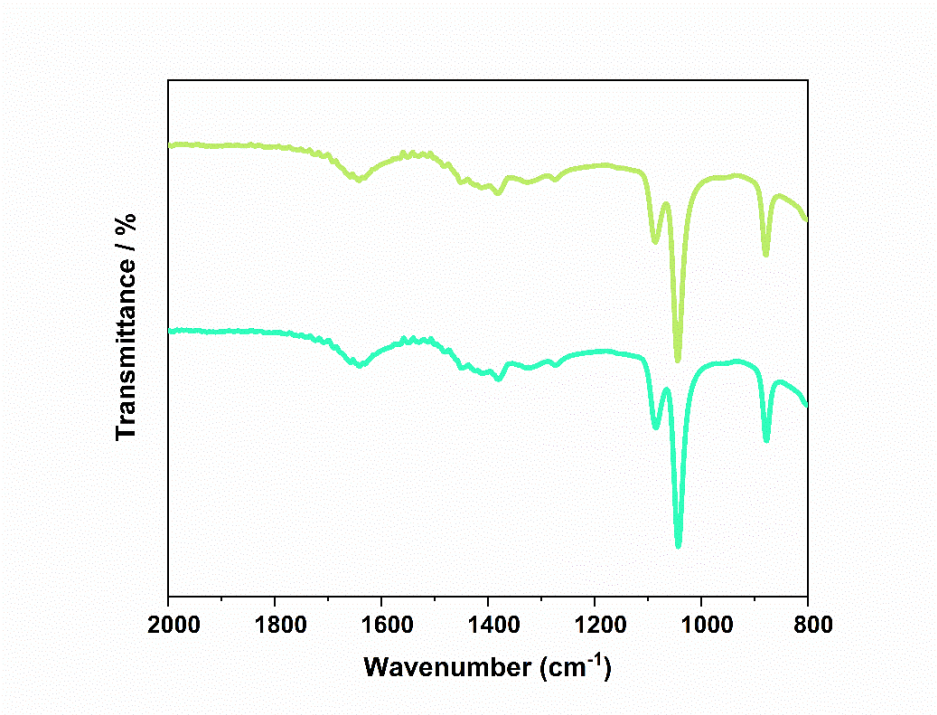

Figure S18. IR spectra of **Pd/(C_2O_4-POM)@rGO** before and after catalysis.

S8 Computational details

Density functional theory (DFT) calculations were performed using the Vienna ab initio package (VASP)[8-11] in virtue of the Perdew-Burke-Ernzerhof (PBE) formulation within the generalized gradient approximation (GGA)[12]. The ion-electron interactions were modeled using the projector-augmented wave (PAW)[13] method. A plane-wave basis was used to expand the Kohn−Sham orbitals, truncated at a kinetic energy of 400 eV. The dispersion-corrected vdW-D3 functional was considered to evaluate the van der Waals effect[14]. The convergence criteria were set to be 10^{-4} eV and 0.03 eV/Å for wavefunction and geometry optimization, respectively. The Brillouin zone integration is performed using 2 × 2 × 1 Monkhorst-Pack k-point sampling for a structure. Periodic images of the slab were separated by at least 15 Å vacuum gap. The electronic density of the structure was processed using VASPKIT[15], and the density derived electrostatic and chemical (DDEC) charges and bond orders of the structure were calculated using the Chargemol software[16,17].

S9 References

1. S. Li, S. Liu, S. Liu, Y. Liu, Q. Tang, Z. Shi, S. Ouyang and J. Ye, $\{Ta_{12}\}/\{Ta_{16}\}$ Cluster-Containing Polytantalotungstates with Remarkable Photocatalytic H_2 Evolution Activity, *J. Am. Chem. Soc.*, 2012, **134**, 19716-19721.
2. M. Filowitz, R. K. C. Ho, W. G. Klemperer, and W. Shum, Oxygen-17 nuclear magnetic resonance spectroscopy of polyoxometalates. 1. Sensitivity and resolution, *Inorg. Chem.,* 1979, **18**, 93-103.
3. W. J. Randall, M. W. Droege, N. Mizuno, K. Nomiya, T. J. R. Weakley, R. G. Finke, Metal Complexes of the Lacunary Heteropolytungstates $[B\text{-}\alpha\text{-}PW_9O_{34}]^{9-}$ and $[\alpha\text{-}P_2W_{15}O_{56}]^{12-}$, *Inorg. Synth.,* 1997, **31**, 167-168.
4. R. Liu, S. Li, X. Yu, G. Zhang, S. Zhang, J. Yao and L. Zhi, A general green strategy for fabricating metal nanoparticles/polyoxometalate/graphene tri-component nanohybrids: enhanced electrocatalytic properties, *J. Mater. Chem.*, 2012, **22**, 3319-3322.
5. K. Guo, L. J. Rowland, L. H. Isherwood, G. Glodan and A. Baidak, Photon-induced synthesis of ultrafine metal nanoparticles on graphene as electrocatalysts: impact of functionalization and doping, *J. Mater. Chem. A*, 2020, **8**, 714-723.
6. G. Sheldrick, A short history of SHELX, *Acta Crystallogr. Section A*, 2008, **64**, 112-122.
7. O. V. Dolomanov, L. J. Bourhis, R. J. Gildea, J. A. K. Howard and H. Puschmann, OLEX2: a complete structure solution, refinement and analysis program, *J. Appl. Cryst.,* 2009, **42**, 339-341.
8. G. Kresse, J. Hafner, Ab initio molecular dynamics for liquid metals, *Phys. Rev. B*, 1993, **47**, 558-561.

9. G. Kresse, J. Hafner, Ab initio molecular-dynamics simulation of the liquid-metal-amorphous-semiconductor transition in germanium, *Phys. Rev. B*, 1994, **49**, 14251-14269.

10. G. Kresse, J. Furthmuller, Efficient Iterative Schemes for Ab Initio Total-Energy Calculations Using a Plane-Wave Basis Set. *Phys. Rev. B,* 1996, **54**, 11169−11186.

11. G. Kresse, J. Furthmuller, Efficiency of Ab-Initio Total Energy Calculations for Metals and Semiconductors Using a Plane-Wave Basis Set. *Comput. Mater. Sci.,* 1996, **6**, 15−50.

12. J. P. Perdew, K. Burke, M. Ernzerhof, Generalized Gradient Approximation Made Simple. *Phys. Rev. Lett.,* 1996, **77**, 3865−3868.

13. G. Kresse, D. Joubert, From Ultrasoft Pseudopotentials to the Projector Augmented-Wave Method. *Phys. Rev. B*, 1999, **59**, 1758−1775.

14. K. Lee, E. D. Murray, L. Kong, B. I. Lundqvist, D. C. Langreth, Higher-accuracy van der waals density functional, *Phys. Rev. B*, 2010, **82**, 081101.

15. V. Wang, N. Xu, J. C. Liu, G. Tang, W. T. Geng, VASPKIT: a user-friendly interface facilitating high-throughput computing and analysis using VASP code, *Comput. Phys. Commun.*, 2021, **267**, 108033.

16. T. A. Manz, N. G. Limas, Introducing DDEC6 atomic population analysis: part 1. Charge partitioning theory and methodology, *RSC. Adv.*, 2016, **6**, 47771-47801.

17. T. A. Manz, Introducing DDEC6 atomic population analysis: part 3. Comprehensive method to compute bond orders, *RSC Adv.*, 2017, **7**, 45552-45581.